De Sio *et al. Micro and Nano Syst Lett (2015) 3:8*
DOI 10.1186/s40486-015-0025-z

Micro and Nano Systems Letters
a SpringerOpen Journal

LETTER Open Access

Photo-thermal effects in gold nanorods/DNA complexes

Luciano De Sio[1,2*], Giulio Caracciolo[3], Ferdinanda Annesi[4], Tiziana Placido[5,6], Daniela Pozzi[3], Roberto Comparelli[6], Alfredo Pane[4], Maria Lucia Curri[6], Angela Agostiano[5,6] and Roberto Bartolino[2,4,7]

Abstract

An ingenious combination of plasmonic nanomaterials and one of the most relevant biological systems, deoxyribonucleic acid (DNA) is achieved by bioconjugating gold nanorods (GNRs) with DNA via electrostatic interaction between positively charged GNRs and negatively charged short DNA. The obtained system is investigated as a function of DNA concentration by means of gel electrophoresis, zeta-potential, DNA melting and morphological analysis. It turns out that the obtained bioconjugated systems present both effective electric charge and aggregate size that are particularly amenable for gene therapy and nanomedicine applications. Finally, the effect of the localized (photo-thermal heating) and delocalized temperature variation on the DNA melting by performing both light induced bio-transparent optical heating experiments and a thermographic analysis is investigated, demonstrating that the developed system can be exploited for monitoring nanoscale temperature variation under optical illumination with very high sensitivity.

Keywords: Nanomaterials, Plasmonics, DNA, Optics, Heat transfer

Background

Gene therapy (GT) has the potential to treat serious human diseases by providing patients with functioning replacements for defective genes or with oligonucleotides that deactivate destructive gene products [1]. GT holds promise for treating a wide range of diseases including cancer, cystic fibrosis, heart disease, diabetes, hemophilia and AIDS. The future use of this type of therapy for clinical applications deals with the manufacturing of appropriate gene delivery vehicles (vectors) with the following capabilities: (1) selective transport of appropriate genes (oligonucleotides) to the diseased tissues; (2) protection of oligonucleotides from physiological degradation (e.g., pH change) while *en route*; presence of an external trigger mechanisms for gene release after the target site is reached. To date the most effective means of GT is based on viral vectors; a tool commonly used by molecular biologists to deliver genetic material into cells [2]. However, viral vectors exhibit some intrinsic drawbacks such as: (1) they can carry only a limited amount of genetic material; (2) they can cause immune responses in patients; (3) the immune system may block the virus from delivering the gene to the patient's cells. Biocompatible gold nanoparticles (GNPs) have gained considerable attention in recent years for potential applications in medicine due to their size dependent electronic, optical and chemical properties [3]. GNPs possess the capability to localize light down to the nanoscale: visible electromagnetic radiation induces an oscillation of the free electrons localized at the metal (NPs)/dielectric (surrounding medium) interface. This phenomenon, called localized plasmon resonance (LPR), can be controlled in frequency by varying both the size and the shape of the nanoparticles and the dielectric constant of the surrounding medium [4]. Plasmonic NPs have also the extraordinary capability to convert external light to heat, as the strong electric field generated around the NPs due to the LPR effect is transformed resulting in nanosized sources of heat [5]. The ability of GNPs to interact with and enter cells has encouraged researchers to attach them various compounds and biological macromolecules [6–8] to gold in an effort to combine

*Correspondence: luciano@beamco.com
[1] Beam Engineering for Advanced Measurements Company, 1300 Lee Road, Orlando, FL 32810, USA
Full list of author information is available at the end of the article

functionality with transport. In particular, GNPs possess a relevant potential as vehicles for gene delivery due to their low cytotoxicity when prepared in suitable size and coated with appropriate ligands. Several strategies have been proposed to bind biological molecules to GNPs [9]. Among the various approaches, use of electrostatic interactions between GNPs and biological molecules offers one of the most viable functionalization route to obtain stable GNP bioconjugates. The convenient assembly of GNPs with suitable biosystems requires that the NP optical activity falls in the first (700–900 nm) or the second (1000–1400 nm) optical window of the NIR region of the electromagnetic spectrum, where the light attenuation by the absorption and scattering from the main tissue constituents (water, lipid, haemoglobin, melanin) is significantly reduced, thus allowing to penetrate biological systems very deeply, down to millimetres and even centimetres scale [10]. Gold nanorods (GNRs) represent an attractive class of GNPs as due to their plasmon absorption sensitivity to the refractive index of the surrounding material, allow for an extremely accurate sensing and make them excellent candidates for biological sensing applications [11]. In addition, GNRs present two distinct LPR, namely transversal and longitudinal ones, which can be tuned up to near-infrared (NIR), thus ensuring their activity in the biological window. Such NIR absorption peaks can be excited by a laser at specific absorption wavelength to induce a local heating, potentially able to selective destroy, via an hyperthermal process, cancerous tissues [12, 13]. Remarkably, the photoinduced thermal effect can be extremely effective in GT procedures, enabling the controlled release of therapeutic oligonucleotides from GNPs [14]. In this paper, a comprehensive study of the electrostatic interaction between an aqueous solution of positively charged GNRs dispersed in a negatively charged short chain DNA solution is reported. A detailed investigation of the characteristics of the obtained bioconjugated has been performed as a function of GNRs concentration based on zeta-potential, gel electrophoresis, dynamic light scattering and morphological analysis. Remarkably, the effect of the localized photo-thermal heating and delocalized temperature variation on the DNA melting in the prepared bioconjugated has been demonstrated. Compared to previously employed techniques [15–17], the proposed non-invasive methodology enables to continuously monitoring photoinduced temperature variations around GNRs with high sensitivity.

General protocol for seed-mediated synthesis of GNRs and their characterization

Cetyltrimethylammonium bromide (CTAB) capped, water dispersible GNRs were synthesized by slight modifying the "seed-mediated growth method" [18]. All glassware used in the following procedures were cleaned in a bath of freshly prepared 3:1 HCl/HNO_3 and rinsed thoroughly in H_2O prior to use. The synthesis was based on a two steps procedure. Firstly, 10 mL of "seed" solution was prepared by mixing CTAB (1 mmol) and $HAuCl_4{\cdot}3H_2O$ (2.5×10^{-3} mmol) at room temperature. Then, 0.6 mL of ice–cold aqueous solution of $NaBH_4$ (0.01 M) were added under vigorous stirring. Upon solution colour turned from greenish-yellow to brown, the mixture was further vigorously stirred for 2 h before utilizing it. In second step, 500 mL of water dispersed CTAB-stabilized GNRs (5.6×10^{-10} M) were grown by dissolving $AgNO_3$, 18.22 g of CTAB and 100 mg of $HAuCl_4{\cdot}3H_2O$. Such mixture was kept at room temperature under continuous stirring. After 3 min, aqueous solution of ascorbic acid (AA) was drop-wise added to the above described mixture in [AA]/[Au] = 2 molar ratio. The resulting solution was kept under stirring until it became colourless [indicative for reduction of Au(III) to Au(I)] [19, 20]. At this point, 0.8 mL of seed solution were added to the growth solution and the resulting mixture was stirred. A brown colour developed in about 30 min. After preparation, GNRs solution was purified from uncoordinated CTAB by means of repeated centrifugation cycles.

Normalized UV–Vis absorption spectrum of GNRs is reported in Fig. 1a. The GNRs dispersion exhibits two typical LPRs: a transverse one at 520 nm and a longitudinal one at 800 nm. The position of longitudinal LPR can be tuned in the VIS–NIR spectral range by carefully tuning the numerous experimental parameters involved in the GNRs preparation, such as purity and concentration of reactants, temperature and specific additives [21]. On the other hand, it is worth mentioning that fundamental for the formation of GNRs is the presence of Ag salt in the reaction mixture [22]. As a matter of fact, a defined amount of Ag^+ ions is crucial for the growth of GNRs up to desired aspect ratio (AR) value. In the investigated case, the molar ratio of [Au]/[Ag] = 5 was used and resulted in GNRs with an AR of about 3.2, as confirmed by TEM (by Jeol JEM-1011 microscope, operating at 100 kV) analysis performed by depositing one droplet of the aqueous GNRs dispersion (Fig. 1b) onto a carbon-coated copper grid, and then allowing the aqueous solvent to evaporate. For a statistical determination of the average GNR size, shape and aspect ratio (AR), at least 200 objects were counted for each sample. The TEM image of Fig. 1c indicates that the particle population consists mainly of GNRs with a 3.2 ± 0.5 AR. Significantly, general protocols for GNRs synthesis typically lead to a yield of 80–90 % in GNRs and a limited contribution of NPs with different shape. In the investigated

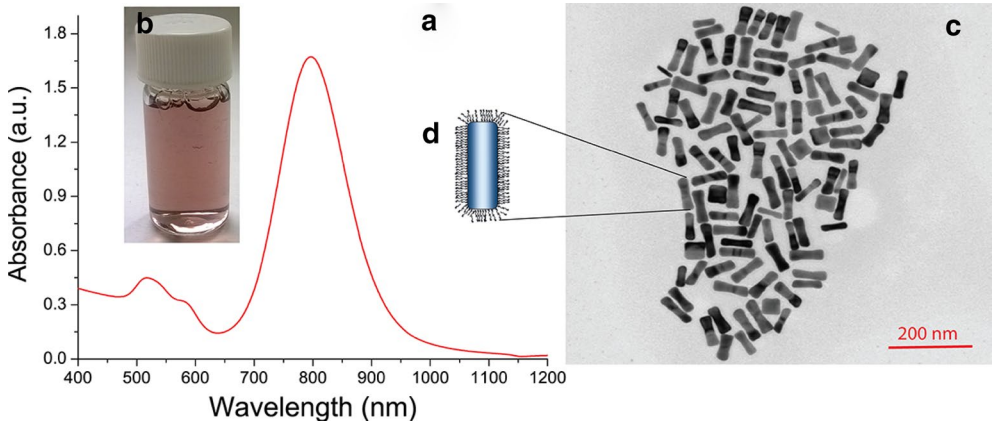

Fig. 1 Normalized UV–Vis absorption spectrum (**a**) for water dispersions of GNRs along with the photo of the vial containing it (**b**). Transmission electron microscopy (TEM) image of the GNRs dispersion (**c**) and schematic representation of a CTAB capped GNR (**d**)

case, the presence of residual particles with a shape other than rod-like, mainly cubes as pointed out by TEM analysis (Fig. 1c), leads to the appearance of a shoulder (at 540 nm) in the spectrum (Fig. 1a) [23].

Macro and micro-electrophoresis experiments

Calf thymus DNA was purchased from Sigma–Aldrich (Alabaster, USA), dissolved in ultrapure water (C_{DNA} = 1 mg/mL) and sonicated for 5 min by ultra-tip-sonication to produce DNA fragments between 500 and 1000 base pairs. For our experiments, GNRs (C = 2.5 10^{-9} M) were incubated with DNA at different GNRs/DNA molar ratios (W = GNRs/DNA base pairs = mol/mol). The range of W (displayed in Fig. 2) has been selected in order to study the complexation of DNA with GNRs in different experimental conditions such as positive, neutral and negative effective electric charge of the system. A preliminary investigation of the interaction between GNRs and DNA was carried out by performing a gel electrophoresis analysis, [24] a technique useful for separation and, sometimes, purification purposed of macromolecules—especially proteins and nucleic acids—that differ in size, charge or conformation. When charged molecules are in an electric field, they migrate toward either the positive or negative pole according to their charge through an agarose matrix. The DNA molecules, being negatively charged along their length, migrate toward the positive electrode, thus resulting separated according to their length during their electrophoretic run, since pores in the agarose matrix allow short DNA molecules to sneak through more easily than the long ones. The different GNRs/DNA mixtures have been doped with a small amount (1 % in weight) of a positively charged blue dye (ethidium bromide, EtBr), which is the most commonly used dye for DNA and RNA detection in gels [25]. EtBr is a DNA intercalator, inserting itself between the base pairs in the double helix. EtBr has UV absorbance maxima at 360 nm and

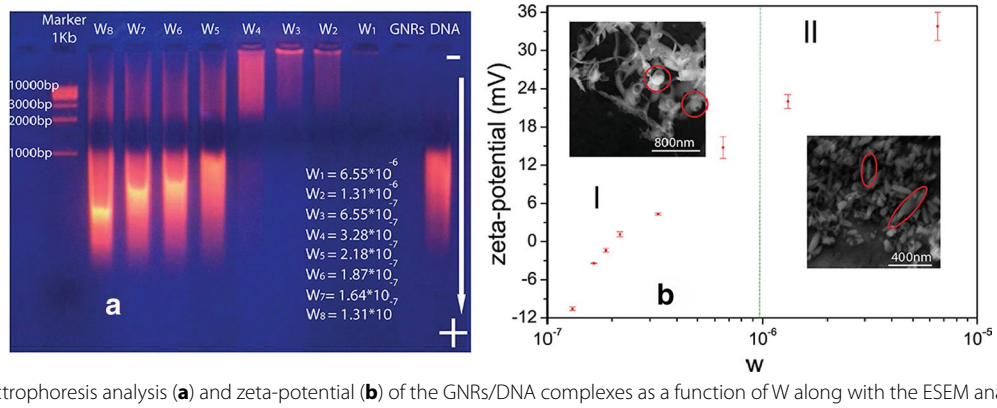

Fig. 2 Gel electrophoresis analysis (**a**) and zeta-potential (**b**) of the GNRs/DNA complexes as a function of W along with the ESEM analysis (*inset* of **b**)

an emission maximum at 590 nm, with its orange fluorescence increasing of about 20 times upon binding to DNA. Later on, the obtained solutions were pipetted in the agarose matrix molded with wells (Fig. 2a), containing also DNA filaments of known size distribution (in the first well on the left of Fig. 2a), which were used as markers. The agarose matrix was then placed on a UV lamp and covered with a UV glass filter. After the power supply was turned on, the DC voltage (120 V, 0.78 mA) induced a migration of the pure DNA (Fig. 2a, first well on the right) towards the positive electrode. The presence of a broad fluorescent band indicated that DNA molecules had fragments between 500 and 1000 base pairs, as anticipated earlier.

Figure 2a (second well on the right) shows that the GNRs dispersion was not affected by the electrophoretic run since GNRs are positively charged due to the presence of the CTAB bilayer. Indeed, GNRs do not exhibit any visible fluorescence band in the well, even in presence of the fluorescent tag (EtBr). The intense fluorescence of EtBr after binding with DNA is probably due to the hydrophobic environment found between the base pairs. By moving into such a hydrophobic environment and away from the solvent (water in our case), the ethidium cation is forced to shed any water molecules that was associated with it. As water is a highly efficient fluorescent quencher, only the removal of water molecules allows the ethidium to fluoresce. On the contrary, no binding event can be thought to occur between GNRs and EtBr and therefore the water based GNRs dispersion represent an effective hydrophobic environment able to induce a strong quenching of the ethidium fluorescence. By increasing the DNA concentration ($W_2 \leq W \leq W_4$) the solution shows a remarkable fluorescence very close to the well, pointing out an inhibited migration toward the positive electrode. Such an evidence can be accounted for by the presence of the CTAB bilayer, which makes GNRs positively charged, and thus able to electrostatically interact with the DNA molecules, without affecting their average length, however changing the effective charge of the whole system. A further increasing in the DNA concentration ($W_5 \leq W \leq W_8$) results in fluorescent bands broader. This evidence can be reasonably explained by thinking that, under these conditions, electrostatic interaction between GNRs and DNA exhibits a saturation and therefore all the non-conjugated DNA molecules or even the over conjugated DNA/GNRs complexes (means complexes with an effective negative electric charge) are free to run towards the positive electrode. Therefore the detected broad are likely due to at the presence of GNRs/DNA complexes with different size and charge (ranging from non-conjugated DNA to over conjugated GNRs/DNA complexes). It is worth mentioning that we have focused our study on the electrostatic interaction between GNRs and DNA (ranging from 500 to 1000 bp). As a matter of fact, it has been reported that the physical–chemical properties of cationic surfactant/DNA complexes are slightly affected by DNA size, while their ability to deliver DNA does [26, 27]. Recent results [28] have demonstrated that delivered DNA facilitated by cationic nanocarriers aggregates to a large extent within the cell, and aggregation is influenced by a number of factors including the location, the environmental conditions, and the DNA size itself. In particular, the smaller DNA sizes exhibited greater aggregation than the larger. Thus, we suggest that DNA size could have a minor effect, if any, on the physical–chemical characterization herein reported, while it could affect intracellular DNA photothermal release and aggregation. This is a key issue that will be addressed in future investigations.

In order to study the effective electric charge of the system, electrophoretic mobility experiments were carried out by means of a laser Doppler electrophoresis technique (Malvern-NanoZetaSizer) [29]. The mobility u was converted into the zeta-potential using the Smoluchowski relation: zeta-potential $=$ $u\eta/\varepsilon$, where ε is the permittivity of the solvent phase while η is the solvent viscosity. Zeta-potential measurements were performed in triplicate and results are reported as average value $\pm$ standard deviation in Fig. 2b. This experiment, realized by measuring the effective electric charge of the system (zeta potential) without adding the EtBr, shows that by increasing the DNA concentration (decreasing W, Fig. 2b*)* the zeta potential decreases. In particular for $W = 2 \times 10^{-7,}$ GNRs/DNA complexes also undergo through a charge inversion effect differentiating negatively and positively charged aggregates. Indeed, this behavior, very similar to the one reported in Fig. 2a (electrophoresis analysis), highlights that the low concentration of EtBr does not affect the overall electric charge of the GNRs/DNA mixtures. As described in details in the Additional file 1 and confirmed by the environmental scanning electron microscope (ESEM) analysis reported in the inset of Fig. 2b for $W < 10^{-6}$ the GNRs/DNA complexes are quasi-spherical clusters (region I), while for $W > 10^{-6}$ their shape is elliptical like (region II). As a result, the GNRs/DNA complexes in region II are simultaneously positively charged and small in size (see Additional file 1). These relevant features make the system a good candidate for drug delivery and GT applications. To this end, it is important to say that the electrostatic interactions are modified in a physiological environment, where ionic strength acts to modify the complex overcharging. Physiological saline solutions have a destabilizing effect on the structure of GNRs/DNA complexes, either when they are prepared

in these solutions or added to them after being prepared in low ionic strength solutions [30, 31]. The presence of salt during complex formation induces a smaller complexation efficiency for each given charge ratio. High salt concentration weakens the association between GNRs and DNA in preformed complexes, with the occurrence of some dissociation.

UV spectroscopy characterization

The effect of the GNRs/DNA conjugation on the overall DNA stability was investigated by performing a thorough spectral characterization of the system and by monitoring the absorption spectrum of the DNA solution, GNRs dispersion and GNRs/DNA complexes as a function of temperature. Absorbance versus temperature profiles were obtained (by means of a computer-interfaced Jasco V-630 spectrophotometer equipped with a thermoelectrically controlled cell holder) by monitoring (at $\lambda = 260$ nm) the intensity of the absorption while heating up (3 °C/min) the samples (DNA solution, GNRs dispersion and GNRs/DNA complexes). The melting temperature (T_m) for each transition was obtained from the optical melting curves by using a previously described procedure [32]. One of the most commonly used and simplest techniques for the DNA melting point determination is spectroscopic analysis by UV absorption. The absorption spectrum is recorded against the dependence of the temperature where the turning point of the graph describes the exact temperature (T_m) at which half of helix structure is lost. In the actual case, the intensity absorption was monitored at $\lambda = 260$ nm since the DNA solution exhibits a well-known sharp maximum at 260 nm due to the absorption of the subunits of nucleic acids (purines and pyrimidines) [33] while the GNRs dispersion does not show any absorbance peak at 260 nm and moreover their overall absorbance does not change with temperature (data not reported). Indeed, high temperature causes DNA to melt due to breaking of hydrogen bonds connecting the bases and, consequently, the absorbance at 260 nm rises (this effect being known as a hyperchromic effect).

Figure 3a shows a typical melting curve of the DNA solution; it exhibits a melting temperature T_m of about 85.0 °C, temperature value in good agreement with previous works [34]. The conjugation of GNRs/DNA acts as a destabilizer for the DNA melting inducing a broader melting transition with a lower T_m values as is evident in Fig. 3b–c. Results are in good agreement with recent findings showing that interaction between DNA and cationic surfactants can result in an increase of UV absorption, and decrease of melting temperature of calf thymus DNA [35]. The melting properties of the GNRs/DNA conjugates were studied in the whole range $W_1 \leq W \leq W_8$, however, here, only the results for two particular values of W (W_2 and W_7) are reported. Indeed, these two values are representative of the explored working range since they are opposite in charge (namely W_2 positive and W_7 negative) and they belong to two distinct regions (W_2, region **II**; W_7 region **I**). It is worth noting that, for the two investigated values of W (W_2, positively charged complexes and W_7, negatively charged complexes) the T_m values are almost the same. The reason can be ascribed to the small difference in the GNRs concentration between W_2 and W_7. As a matter of fact, we did not investigate the behavior of T_m outside the selected working range ($W_1 \leq W \leq W_8$) since it is meaningless for the goal of our applications.

Plasmonic photo-thermal heating

The influence on the DNA melting of local heating induced by a bio-transparent optical radiation, through the GNRs resonance was investigated by means of a set of all-optical experiments performed by using the all-optical setup reported in Fig. 4. This setup profits of a collimated white source (240 nm < λ < 850 nm) for monitoring the spectral properties of the GNRs/DNA solution and a CW NIR pump laser emitting at $\lambda = 800$ nm ($P_{pump} = 0.14$ W/cm^2) in the high absorption range

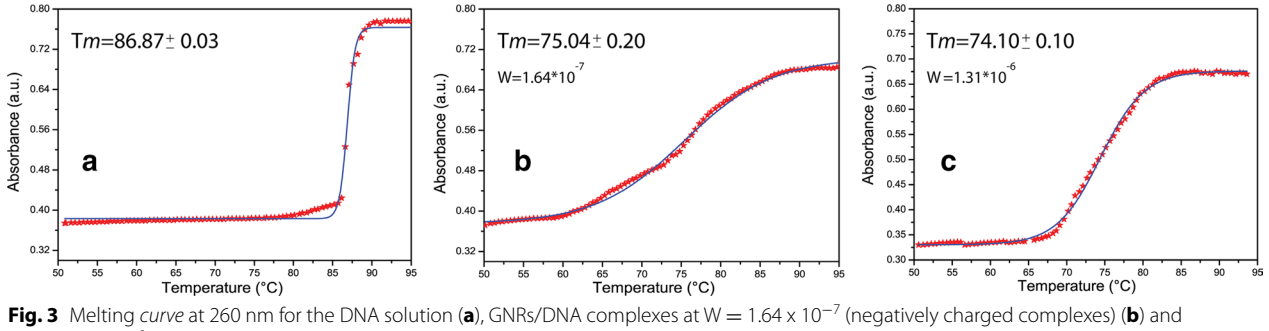

Fig. 3 Melting *curve* at 260 nm for the DNA solution (**a**), GNRs/DNA complexes at W = 1.64 x 10^{-7} (negatively charged complexes) (**b**) and W = 1.31 x 10^{-6} (positively charged complexes) (**c**). The *solid line* is the best sigmoidal fit to the data

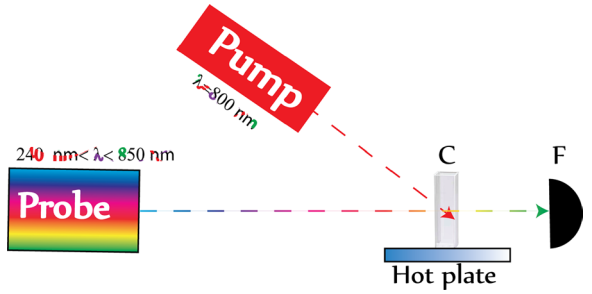

Fig. 4 All-optical setup for sample characterization. *F* is the transmission optical fiber

(longitudinal band) of the GNRs. The sample is placed on a hot plate for control experiments based on delocalized/uniform heat.

The photo-heating experiments was carried out on both W_2 and W_7 GNRs/DNA solutions but, due to the low concentration of GNRs, no significant result was detected in the W_7 solution and therefore all the experiments reported here were performed on the W_2 solution.

Figure 5a (red curve) shows the absorption spectrum of the sample. Remarkably three distinctive markers of GNR absorption, namely transverse and longitudinal LPRs, at 520 and 800 nm respectively, and the DNA absorption peak at $\lambda = 260$ nm, can be identified. By optically pumping the same probed sample area, the photoexcitation of GNRs induces an electric-driven Joule heating with a consequent energy exchange with the surrounding medium (DNA in our case) [36].

This local-heating induces a gradually DNA melting (Fig. 5a, from blue to black curve) with a consequent enhancement of the absorption peak at 260 nm according with the mechanism previously described. It turns out that plot of the intensity of the DNA absorption peak versus the illumination time exhibits a linear behavior (Fig. 5b). Moreover, the refractive index change of the DNA under optical illumination induces a small blue shift of the longitudinal plasmon GNRs at 800 nm (5–6 nm) blue shift while no shift can be detected for the transverse band at 520 nm. This behaviour can be explained by considering that the sensitivity of the LPR wavelength (λ_{LPR}) with respect to the refractive index of

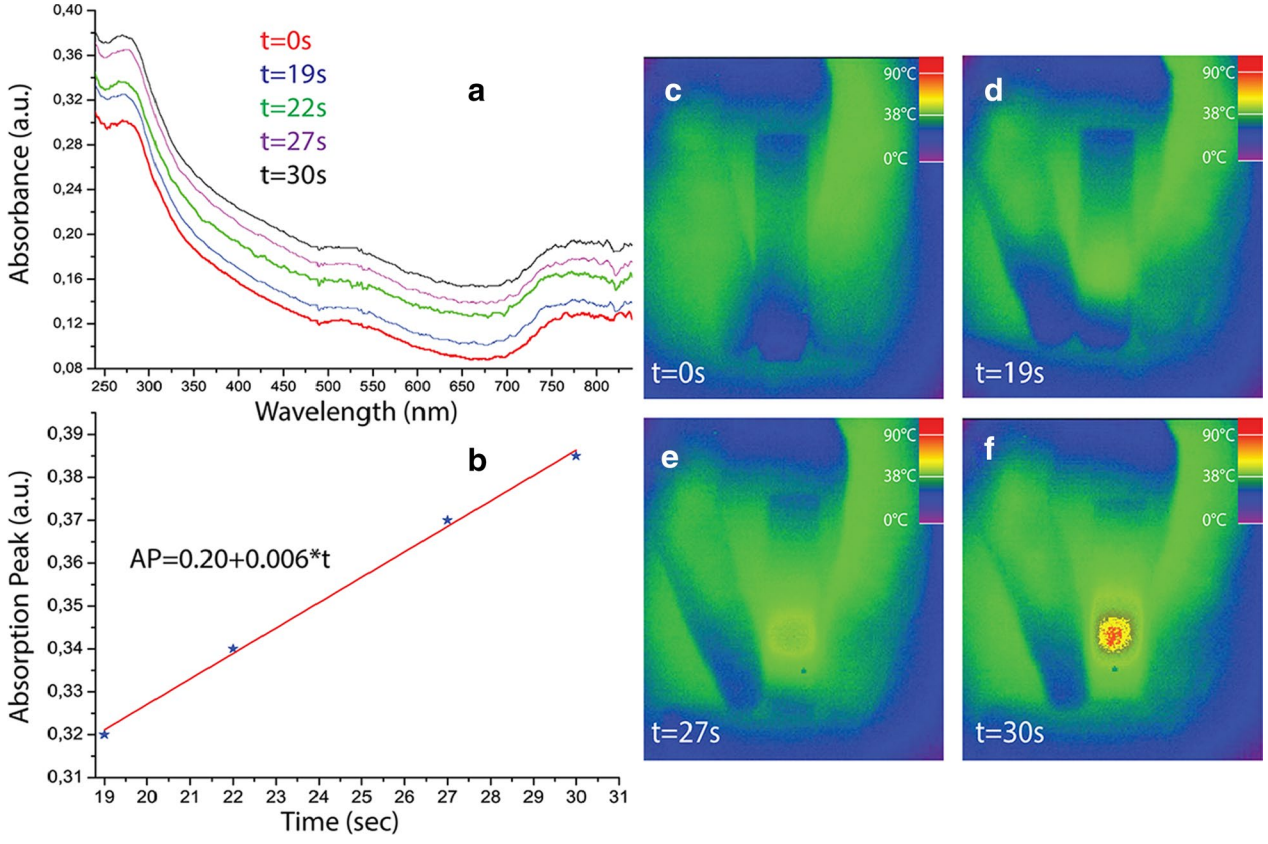

Fig. 5 Absorption spectra of the sample for different values of illumination time (**a**) and linear fit of the intensity of the DNA absorption peak (at $\lambda = 260$ nm) versus the illumination time (**b**). Thermographic analysis of the sample for different illumination times (**c**–**f**)

the surrounding medium (n_s) can be expressed as [37, 38]:

$$\frac{d\lambda_{LPR}}{dn_s} \prec \lambda_P AR \quad (1)$$

where λ_p is the bulk plasma wavelength of gold and AR is the aspect ratio of nanorods. Equation 1 clearly shows that the sensitivity of the LPR wavelength is linearly proportional to AR and λ_p. In the actual case, since AR is 3.2 for the longitudinal band while is 1 (spherical like case) for the transverse band it is easy to understand why there is a low sensitivity of the transverse band to variation of the refractive index of the surrounding medium, while a concomitant high sensitivity is observed for the longitudinal plasmon band. Figure 5c–f shows the thermographic analysis of the sample for different illumination times. The experiments were realized by keeping the hand fingers close to the sample (in our case the GNRs/DNA solution is inside a 2 × 10 mm UV–Vis quartz cuvette) in order to have a bio-setpoint (T ≈ 37 °C). The thermographic analysis shows that the surface of the illuminated area is photo-heated with a temperature variation ranging from 25 °C up to 90 °C meanwhile the bio-setpoint is kept at the same temperature (T ≈ 37 °C). It is worth saying that the thermo-camera can measure the temperature with high accuracy (≈0.5 °C) only at the focal plane and for this reason, with this technique, it is possible to measure the temperature of the GNRs/DNA solution only on the front face of the cuvette.

A validation of the effect of the GNRs induced local heating on the DNA, was achieved by performing a control experiment by varying the sample temperature from 25 °C up to 95 °C and monitoring the absorption spectrum (Fig. 6a). The delocalized heating was found, once more, to induce a gradual DNA melting with a consequent enhancement of the absorption peak at 260 nm, thus confirming that the photo-thermal nature of the behavior reported in Fig. 5a. It is worth noting that the two calibration functions reported in Figs. 5b and 6b, within the experimental error, exhibit the same linear behavior. Therefore, by using the linear function reported in Fig. 6b, it is possible to calculate the average temperature of the sample by means of the following equation:

$$T = \frac{(AP - 0.142)}{0.0061}$$

This result shows that it is possible to measure the average temperature around GNRs at a given illumination time with a sensitivity of about 0.06 °C by simply monitoring the intensity of the absorption peak at 260 nm. Remarkably the presented method offer an original tool to monitor nanoscale temperature variation in a biocompatible environment by exploiting the DNA melting process. In order to visualize the difference between localized (confined to the illuminated area) and delocalized (uniform) temperature variation, the temperature of the GNRs/DNA solution was measured by heating up the quartz cuvette with a hot plate, the investigated area is marked with a white circle in Fig. 6. As a result (Fig. 6c–f), the heating transfer from the plate to the cuvette results in a quite uniform temperature distribution along the surface of the cuvette, clearly pointing out the difference between localized (generated by light) and delocalized (generated by a hot plate) temperature variation. This "visual comparison" based on a thermographic analysis is a proof-of-concept that in case of in vivo applications (e.g., GT or photo-thermal therapy) only the illuminated area is photo-heated (e.g., cancer cells) while the surrounding medium is not affected (e.g., healthy cells). Conversely, in case of heat generated through magnetic therapy (delocalized heat) the whole sample area is affected by the treatment (e.g., both cancer and healthy cells). Moreover, the localized heat can be used for photothermal release of DNA from GNRs for GT applications. It is worth mentioning that the reported method has been investigated in a temperature range between 72 and 85 °C (or irradiation time between 19 and 30 s) in order to study the photo-induced melting properties of the DNA solution. However, the same approach can be extended to other, lower, temperature range (e.g., 25–72 °C), by using a different calibration curve since the full melting diagram of a DNA solution exhibits a sigmoidal behavior, due to superimposition of two linear calibration curves (see Fig. 3). Above 85 °C, since all the double-stranded DNA unwinds and separates into single-stranded DNA, the melting curve exhibits a saturation region (see Fig. 3). For this reason, there is no physical meaning for studying the photo-thermal properties of the DNA/GNRs solution beyond 30 s.

Conclusion

A detailed study has been reported on the electrostatic interaction between a GNRs dispersion and a DNA solution. Both effective electrostatic charge and average size/shape can be easily controlled by carefully selecting the suitable GNRs/DNA molar ratio. In particular, the GNRs/DNA complexes also undergo through a charge inversion effect, finally differentiating negatively and positively charged conjugates. These distinctive features make them promising candidates for drug delivery and GT applications both in vitro and in vivo [39]. Photo-heating experiments realized through a bio-transparent optical radiation (λ = 800 nm) demonstrated that the system represent an accurate temperature sensor able to monitor heating variation trough the DNA melting (at λ = 260 nm) with a sensitivity of about 0.06 °C. The

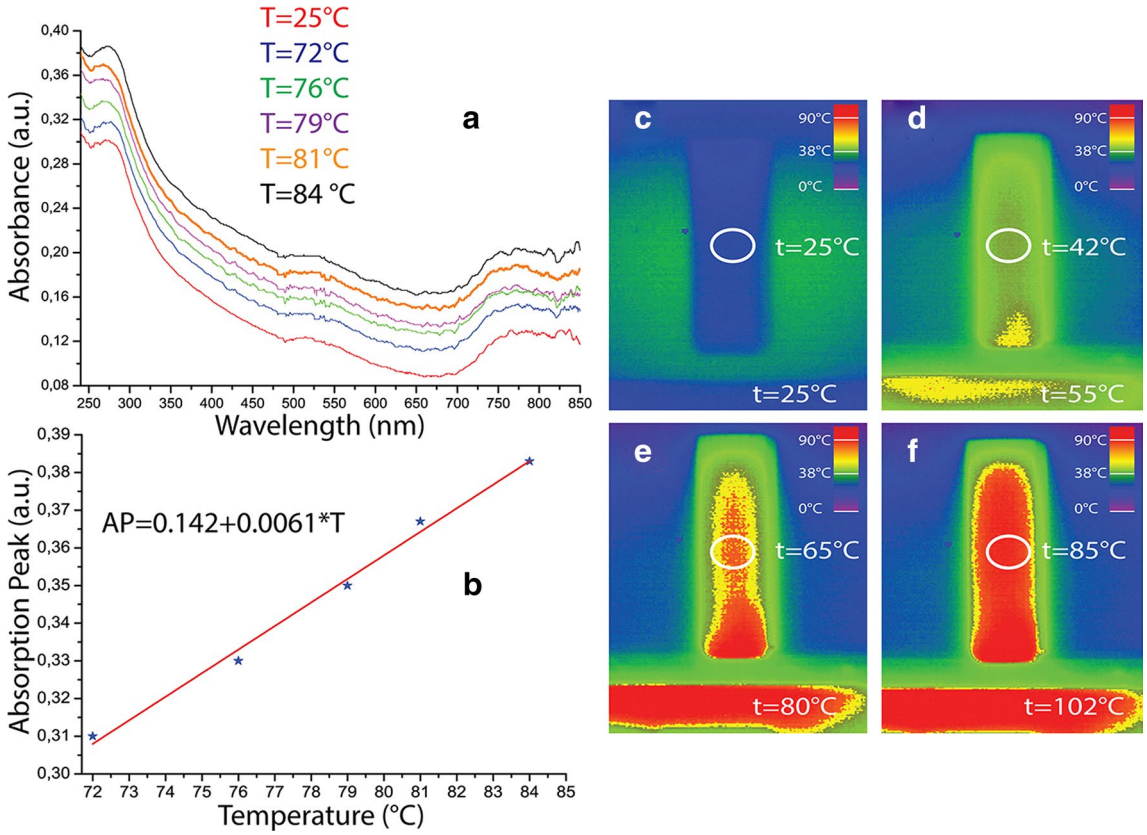

Fig. 6 Absorption spectra of the sample for different values of temperature (**a**) and linear fit of the intensity of the DNA absorption peak (at $\lambda = 260$ nm) versus the temperature (**b**). Thermographic analysis of the sample for different temperatures (**c**–**f**)

overall results allow a deeper fundamental understanding of the interaction between charged plasmonic and biological materials [40] and, at the same time, open-up the venue for realizing a new generation of tools for nanomedicine.

Additional file

Additional file 1. Dynamic Light Scattering experiments

Authors' contributions

LD, GC, RB conceived the photo-thermal strategy in GNRs/DNA complexes. LD performed the photo-heating experiments, GC and DP performed the zeta-potential and DNA melting experiments, FA and AP realized the gel electrophoresis analysis, TP realized the synthesis of GNRs, RC performed the TEM analysis, MLC and AA supplied background of GNRs synthesis and optical characterization, RB supplied background of photo-thermal heating of GNRs and DNA characterization. LD, GC wrote the paper. All authors read and approved the final manuscript.

Author details

[1] Beam Engineering for Advanced Measurements Company, 1300 Lee Road, Orlando, FL 32810, USA. [2] Department of Physics, University of Calabria Centre of Excellence for the Study of Innovative Functional Materials, 87036 Arcavacata Di Rende, Italy. [3] Dipartimento di Medicina Molecolare, Sapienza Università di Roma, Viale Regina Elena 291, 00161 Rome, Italy. [4] CNR-IPCF UOS Cosenza, 87036 Arcavacata Di Rende, Italy. [5] Università degli Studi di Bari-Dip. Chimica, Via Orabona 4, 70126 Bari, Italy. [6] CNR-IPCF Istituto per i Processi Chimici e Fisici, Sez. Bari, c/o Dip. Chimica, Via Orabona 4, 70126 Bari, Italy. [7] Interdisciplinary Institute B, Segre of the National Academy dei Lincei, 00165 Rome, Italy.

Acknowledgements

Authors are grateful to: Dr. Giovanni Desiderio for performing the ESEM analysis. The research is supported by the Air Force Office of Scientific Research (AFOSR), Air Force Research Laboratory (AFRL), U.S. Air Force, under grant FA9550-14-1-0050 (P.I. L. De Sio, EOARD 2014/2015) and the Materials and Manufacturing Directorate, AFRL; by 2011 - prot. 2010C4R8M8 and 2012 prot. 2012T9XHH7 PRIN Projects. Fundings have been generously provided to GC by the "Futuro in Ricerca 2008" program funded by the Italian Minister for University and Research (Grant No. RBFR08TLPO) and by the Istituto Italiano di Teconologia, Center for Life Nano Science@Sapienza.

Competing interests

The authors declare that they have no competing interests.

Received: 21 July 2015 Accepted: 29 September 2015
Published online: 12 October 2015

References

1. Friedmann T (1992) A brief history of gene therapy. Nat Genet 2:93–98
2. Cao S, Cripps A, Wei MQ (2010) New strategies for cancer gene therapy: progress and opportunities. Clin Exp Pharmacol Physiol 37:108–114
3. Liz-Marzan LM (2004) Nanometals: formation and color. Mater Today 7:26–31

4. Su KH, Wei QH, Zhang X, Mock JJ, Smith DR, Schultz S (2003) Interparticle coupling effects on plasmon resonances of nanogold particles. Nano Lett 3:1087–1090
5. Ekici O, Harrison RK, Durr NJ, Eversole DS, Lee M, Ben-Yakar A (2008) Thermal analysis of gold nanorods heated with femtosecond laser pulses. J Phys D Appl Phys 41:185501
6. Azzazy HM, Mansour MMH (2009) In vitro diagnostic prospects of nanoparticles. Clin Chim Acta 403:1–8
7. Brigger I, Dubernet C, Couvreur P (2002) Nanoparticles in cancer therapy and diagnosis. Adv Drug Deliv Rev 54:631–651
8. Boisselier E, Astruc D (2009) Gold nanoparticles in nanomedicine: preparations, imaging, diagnostics, therapies and toxicity. Chem Soc Rev 38:1759–1782
9. Barhoumi A, Huschka R, Bardhan R, Knight MW, Halas NJ (2009) Light-induced release of DNA from plasmon-resonant nanoparticles: towards light-controlled gene therapy. Chem Phys Lett 482:171–179
10. Simpson CR, Kohl M, Essenpreis M, Copey M (1998) Near-infrared optical properties of ex vivo human skin and subcutaneous tissues measured using the Monte Carlo inversion technique. Phys Med Biol 43:2465–2478
11. De Sio L, Klein G, Serak S, Tabiryan N, Cunningham A, Tone CM, Ciuchi F, Bürgi T, Umeton C, Bunning T (2013) All-optical control of localized plasmonic resonance realized by photoalignment of liquid crystal. J Mater Chem C 1:7483–7487
12. Huang X, Jain PK, El Sayed IH, El-Sayed MA (2008) Plasmonic photothermal therapy (PPTT) using gold nanoparticles. Lasers Med Sci 23:217–228
13. Bardhan R, Lal S, Joshi A, Halas N (2011) Theranostic nanoshells: from probe design to imaging and treatment of cancer. J Acc Chem Res 44:936–946
14. Huschka R, Zuloaga J, Knight MW, Brown LV, Nordlander P, Halas NJ (2011) Light-induced release of DNA from gold nanoparticles: nanoshells and nanorods. J Am Chem Soc 133:12247–12255
15. Richardson HH, Hickman ZN, Govorov AO, Thomas AC, Zhang W, Kordesch ME (2006) Thermooptical properties of gold nanoparticles embedded in ice: characterization of heat generation and melting. Nano Lett 6:783–788
16. Wilson OM, Hu X, Cahill DG, Braun PV (2002) Colloidal metal particles as probes of nanoscale thermal transport in fluids. Phys Rev B 66:224301–224306
17. Biswal SL, Raorane D, Chaiken A, Birecki H, Majumdar A (2006) Nanomechanical detection of DNA melting on microcantilever surfaces. Anal Chem 78:7104–7109
18. Khanal BP, Zubarev ER (2007) Rings of nanorods. Angew Chem Int Ed Engl 46:2195–2198
19. Pérez-Juste J, Pastoriza-Santos I, Liz-Marzán LM, Mulvaney P (2005) Gold nanorods: synthesis, characterization and applications. Coord Chem Rev 249:1870–1901
20. Placido T, Comparelli R, Giannici F, Cozzoli PD, Capitani G, Striccoli M, Agostiano A, Curri ML (2009) Photochemical synthesis of water-soluble gold nanorods: the role of silver in assisting anisotropic growth. Chem Mater 21:4192–4202
21. Jiang XC, Brioude A, Pileni MP (2006) Gold nanorods: limitation in their syntheses and optical properties. Colloid Surf A Physicochem Eng Asp 277:201–206
22. Giannici F, Placido T, Curri ML, Striccoli M, Agostiano A, Comparelli R (2009) The fate of silver ions in the photochemical synthesis of gold nanorods: an extended X-ray absorption fine structure analysis. Dalton Trans 46:10367–10374
23. Ringe E, McMahon JM, Sohn K, Cobley C, Xia Y, Huang J, Schatz GC, Marks LD, Van Duyne RP (2010) Unraveling the effects of size, composition, and substrate on the localized surface plasmon resonance frequency of gold and silver nanocubes: a systematic single particle approach. J Phys Chem C 114:12511–12516
24. Lee PY, Costumbrado J, Hsu CY, Kim YH (2012) Agarose gel electrophoresis for the separation of DNA fragments. J Vis Exp 20:3923
25. LePecq JB, Paoletti C (1967) A fluorescent complex between ethidium bromide and nucleic acids. Physical–chemical characterization. J Mol Biol 27:87–106
26. Kreiss P, Cameron B, Rangara R, Mailhe P, Aguerre-Charriol O, Airiau M, Scherman D, Crouzet J, Pitard B (1999) DNA size does not affect the physicochemical properties of lipoplexes but modulates gene transfer efficiency. Nucleic Acids Res 27:3792–3798
27. Caracciolo G, Pozzi D, Caminiti R, Marchini C, Montani M, Amenitsch H (2008) Effect of pH on the structure of lipoplexes. J Appl Phys 104:014701–014705
28. Mieruszynski S, Briggs C, Digman MA, Gratton E, Jones MR (2015) Live cell characterization of DNA aggregation delivered through lipofection. Sci Rep 5:1–8
29. Caracciolo G, Pozzi D, Capriotti AL, Marianecci C, Carafa M, Marchini C, Montani M, Amici A, Amenitsch H, Digman MA, Gratton E, Sanchez SS, Laganà A (2011) Factors determining the superior performance of lip id/DNA/protammine nanoparticles over lipoplexes. J Med Chem 54:4160–4171
30. Pozharski E, MacDonald RC (2003) Lipoplex thermodynamics: determination of DNA-cationic lipoid interaction energies. Biophys J 85:3969–3978
31. Zhang Y, Garzon-Rodriguez W, Manning MC, Anchordoquy TJ (2003) The use of fluorescence resonance energy transfer to monitor dynamic changes of lipid-DNA interactions during lipoplex formation. Biochim Biophys Acta 1614:182–192
32. Marky LA, Kallenbach NR, McDonough KA, Seeman NC, Breslauer KJ (1987) the melting behavior of a nucleic acid junction: a calorimetric and spectroscopic study. Biopolymers 26:1621–1634
33. Sinden RR (1994) DNA Structure and Function. Academic Press, San Diego
34. Marmur J, Doty P (1962) Determination of base composition of deoxyribonucleic acid from its thermal denaturation temperature. J Mol Biol 5:109–118
35. Hianik T, Wang X, Tashlitsky V, Oretskaya T, Ponikova S, Antalík M, Ellis JS, Thompson M (2010) Interaction of cationic surfactants with DNA detected by spectroscopic and acoustic wave techniques. Analyst 135(5):980–986
36. De Sio L, Placido T, Comparelli R, Curri L, Striccoli M, Tabiryan N, Bunning T (2015) Next-generation thermo-plasmonic technologies and plasmonic nanoparticles in optoelectronics. Prog Quantum Electron 41:23–70
37. Tian L, Gandra Chen E, Abbas A, Singamaneni S (2012) Gold nanorods as plasmonic nanotransducers: distance-dependent refractive index sensitivity. Langmuir 28:17435–17442
38. De Sio L, Placido T, Serak S, Comparelli R, Tamborra M, Tabiryan N, Curri ML, Bartolino R, Umeton C, Bunning T (2013) Nano-localized heating source for photonics and plasmonics. Adv Opt Mater 1:992
39. Albanese A, Tang PS, Chan WCW (2012) The effect of nanoparticle size, shape, and surface chemistry on biological systems. Annu Rev Biomed Eng 14:1–16
40. De Sio L, Annesi F, Placido T, Comparelli R, Bruno V, Pane A, Palermo G, Curri L, Umeton C, Bartolino R (2015) Templating gold nanorods with liquid crystalline DNA. J Opt 17:025001–025006